# A Unified View of Ethylene Polymerization by $d^0$ and $d^0f^n$ Transition Metals. Part 2: Chain Propagation

**Peter Margl, Liqun Deng, and Tom Ziegler***

*Contribution from the Department of Chemistry, University of Calgary, 2500 University Drive, N.W., T2N 1N4 Calgary, Alberta, Canada*

*Received December 12, 1997. Revised Manuscript Received March 31, 1998*

**Abstract:** We present a systematic investigation of chain propagation by ethylene insertion into the $M-C_2H_5$ bond for a number of $d^0$ [L]M-$C_2H_5$(0,+,2+)-fragments (M = Sc(III), Y(III), La(III), Lu(III), Ti(IV), Zr(IV), Hf(IV), Ce(IV), Th(IV), and V(V); L = NH-$(CH)_2$-$NH^{2-}$ [1], N$(BH_2)$-$(CH)_2$-$(BH_2)N^{2-}$ [2], O-$(CH)_3$-$O^-$ [3], $Cp_2^{2-}$ [4], NH-Si$(H_2)$-$C_5H_4^{2-}$ [5], [(oxo)(O-$(CH)_3$-O)]$^{3-}$ [6], $(NH_2)_2^{2-}$ [7], $(OH)_2^{2-}$ [8], $(CH_3)_2^{2-}$ [9], NH-$(CH_2)_3$-$NH^{2-}$ [10], and O-$(CH_2)_3$-$O^{2-}$ [11]). For sterically unencumbered systems [L]$MC_2H_5^+(C_2H_4)$ (L = 7, 8, 9), it is shown that front-side (FS) ethylene insertion barriers follow the order Sc < Y < La and Ti < Zr < Hf. Insertion barriers for group 3 metals are usually lower than those for group 4 metals. The origin of this trend is in the aptitude of the [L]$MC_2H_5^{n+}$ framework to occupy trigonal planar arrangement, which previously was shown to follow the trend Sc > Y > La > Ti > Zr > Hf. Backside (BS) insertion barriers, on the other hand, depend little on the identity of the metal center as BS insertion requires little deformation of the metal−ligand framework. For these sterically unencumbered systems, it is found that the insertion reaction proceeds through FS and BS channels in equal parts since FS- and BS-transition states are close in energy. Ligand influence on insertion barriers is such that good $\pi$-donor ligands such as [7] lower the front-side insertion barrier, as they favor trigonal planar over trigonal pyramidal coordination. The activity of different metal centers can be drastically changed by sterically bulky ligands. Steric bulk generally tends to lower insertion barriers, since compression of the active site favors the transition state geometry over the $\pi$-complex geometry.

## Introduction

As the commercial importance of polyolefin production by homogeneous Ziegler−Natta-type catalysis continues to increase, the prospect of setting up a set of rules for the construction of successful catalyst systems becomes ever more attractive. Although experimental results have not yet led to a unified set of rules that could be used to construct novel catalysts, recent experiments have revealed that the family of single-site olefin polymerization catalysts is actually much larger than one would have expected a few years ago. Also, those experiments make it likely that it extends across the periodic table, involving not only early transition metals but also late ones such as Ni(II),[1] Pd(II),[2] and Co(III).[3] Much experimental[4−21] and theoretical[22−33] effort is, however, still devoted to $d^0$ transition metal systems, with a focus on the group 4 metals Ti, Zr, and Hf.

As part of a project to set up a theoretical framework for single site polymerization, the present series of papers attempts to develop a unified description of $d^0$-metal-catalyzed Ziegler−Natta olefin polymerization. The prequel of the present study[34] described the energetics of the metal−ligand framework and of ethylene uptake. Building upon these results, the present paper develops rules for predicting the speed of the actual chain propagation step, based on a sample of 45 catalysts of the general composition [L]M-$C_2H_5^{(0,+,2+)}$-fragments (M = Sc-(III), Y(III), La(III), Lu(III), Ti(IV), Zr(IV), Hf(IV), Ce(IV),

(1) Killian, C. M.; Tempel, D. J.; Johnson, L. K.; Brookhart, M. *J. Am. Chem. Soc.* **1996**, *118*, 11664.
(2) Rix, F. C.; Brookhart, M.; White, P. S. *J. Am. Chem. Soc.* **1996**, *118*, 4746.
(3) Brookhart, M.; DeSimone, J. M.; Tanner, M. J. *Macromolecules* **1995**, *28*, 5378.
(4) Scollard, J. D.; McConville, D. H. *J. Am. Chem. Soc.* **1996**, *118*, 10008.
(5) Scollard, J. D.; McConville, D. H.; Payne, N. C.; Vittal, J. J. *Macromolecules* **1996**, *29*, 5241.
(6) Shah, S. A. A.; Dorn, H.; Voigt, A.; Roesky, H.; Parisini, E.; Schmidt, H.-G.; Noltemeyer, M. *Organometallics* **1996**, *15*, 3176.
(7) Fokken, S.; Spaniol, T. P.; Kang, H.-C.; Massa, W.; Okuda, J. *Organometallics* **1996**, *15*, 5069.
(8) van der Linden, A.; Schaverien, C. J.; Meijboom, N.; Ganter, C.; Orpen, A. G. *J. Am. Chem. Soc.* **1995**, *117*, 3008.
(9) Warren, T. H.; Schrock, R. R.; Davis, W. M. *Organometallics* **1996**, *15*, 562.
(10) Brand, H.; Capriotti, J. A.; Arnold, J. *Organometallics* **1994**, *13*, 4469.
(11) Tjaden, E. B.; Swenson, D. C.; Jordan, R. F.; Petersen, J. L. *Organometallics* **1995**, *14*, 371.
(12) Horton, A. D.; de With, J.; van der Linden, A. J.; van de Weg, H. *Organometallics* **1996**, *15*, 2672.
(13) Fuhrmann, H.; Brenner, S.; Arndt, P.; Kempe, R. *Inorg. Chem.* **1996**, *35*, 6742.
(14) Cozzi, P. G.; Gallo, E.; Floriani, C.; Chiesi-Villa, A.; Rizzoli, C. *Organometallics* **1995**, *14*, 4994.
(15) Cloke, F. G. N.; Geldbach, T. J.; Hitchcock, P. B.; Love, J. B. *J. Organomet. Chem.* **1996**, *506*, 343.
(16) Uhrhammer, R.; Black, D. G.; Gandner, T. G.; Olsen, J. D.; Jordan, R. F. *J. Am. Chem. Soc.* **1993**, *115*, 8493.
(17) Long, D. P.; Bianconi, P. A. *J. Am. Chem. Soc.* **1996**, *118*, 12453.
(18) Aoyagi, K.; Gantzel, P. K.; Kalai, K.; Tilley, T. D. *Organometallics* **1996**, *15*, 923.
(19) Jia, L.; Yang, X.; Stern, C.; Marks, T. J. *Organometallics* **1994**, *13*, 3755.
(20) Murphy, V. J.; Turner, H. *Organometallics* **1997**, *16*, 2495.
(21) Antonelli, D. M.; Leins, A.; Stryker, J. M. *Organometallics* **1997**, *16*, 2500.
(22) Janiak, C. *J. Organomet. Chem.* **1993**, *452*, 63.

S0002-7863(97)04213-3 CCC: $15.00 
Published on Web 05/20/1998

**Scheme 1**

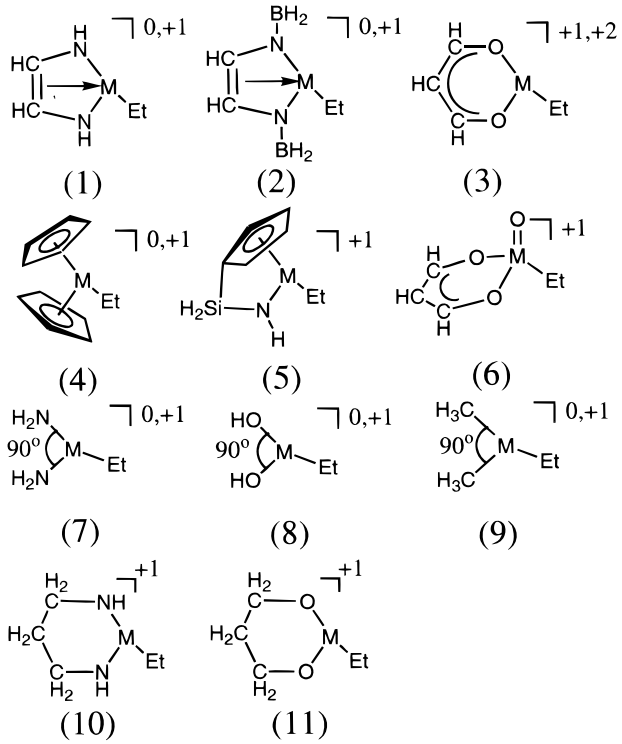


Th(IV), and V(V); L = NH-$(CH)_2$-$NH^{2-}$ [1], N$(BH_2)$-$(CH)_2$-$(BH_2)N^{2-}$ [2], O-$(CH)_3$-$O^-$ [3], $Cp_2^{2-}$ [4], NH-Si$(H_2)$-$C_5H_4^{2-}$ [5], [(oxo)(O-$(CH)_3$-O)]$^{3-}$ [6], $(NH_2)_2^{2-}$ [7], $(OH)_2^{2-}$ [8], $(CH_3)_2^{2-}$ [9], NH-$(CH_2)_3$-$NH^{2-}$ [10], and O-$(CH_2)_3$-$O^{2-}$ [11] (Scheme 1).

Activity and polymer specifications achieved by a given polymerization catalyst depend on a great variety of factors, some of which are not even related to the catalyst itself but to a counterion or a solvent. Nevertheless, it is a necessary condition for a serviceable catalyst to have a high intrinsic aptitude toward the so-called "chain propagation" step and a low aptitude toward all competing "chain termination" processes. As shown in Scheme 2, the chain propagation process for Ziegler-type catalysts is initiated by olefin uptake (a) followed by an insertion reaction b between the metal−polymer bond and the incoming olefin. The often-dominant competing process is transfer of a polymer $\beta$-hydrogen atom to the approaching olefin (c), leading to termination of the chain and regrowth of a new chain, after the terminated chain has been

**Scheme 2**

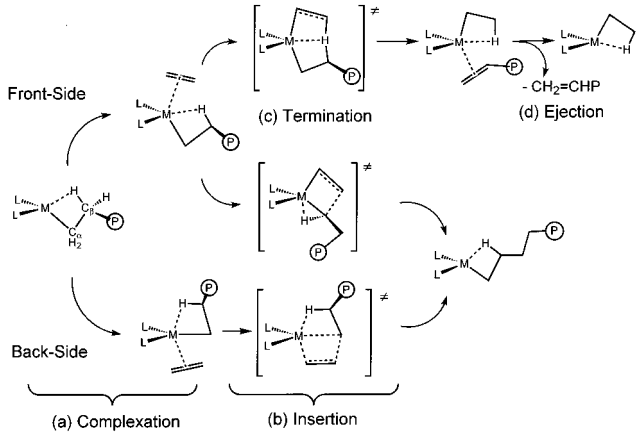


ejected (d). In the present study, we describe the essential step for olefin polymerization activity, (b). As in the predecessor to this study, we explicitly do not consider steric hindrance deriving from large substituents, since it is our aim to outline the influence of the metal and the first coordination sphere on olefin complexation and insertion energetics. Exceptions to this are sterically bulky ligands that form an irreducible entity such as in $(Cp)_2$.

Unless otherwise stated, we use an ethyl group as a model for the growing polymer chain, a measure which has been rationalized in previous publications[35,36] and which represents an optimum choice to balance physical accuracy and computing resources.

## Computational Details

Stationary points on the potential energy surface were calculated with the program ADF, developed by Baerends et al.,[37,38] and vectorized by Ravenek.[39] The numerical integration scheme applied for the calculations was developed by te Velde et al.[40,41] The geometry optimization procedure was based on the method due to Versluis and Ziegler.[42] The frozen core approximation was employed thoughout. The electronic configurations of the molecular systems were described by a triple-$\zeta$ Slater-type basis set on metal atoms and by a double-$\zeta$ quality basis on nonmetal atoms (see Supporting Information for details).[43,44] A set of auxiliary[45] s, p, d, f, and g STO functions, centered on all nuclei, was used to fit the molecular density and present Coulomb and exchange potentials accurately in each SCF cycle. Energy differences were calculated by augmenting the local exchange-correlation potential by Vosko et al.[46] with Becke's[47] nonlocal exchange

(23) Jolly, C. A.; Marynick, D. S. *J. Am. Chem. Soc.* **1989**, *111*, 7968.
(24) Castonguay, L. A.; Rappe, A. K. *J. Am. Chem. Soc.* **1992**, *114*, 5832.
(25) Prosenc, M.; Janiak, C.; Brintzinger, H. H. *Organometallics* **1992**, *11*, 4036.
(26) Kawamura-Kuribayashi, H.; Koga, N.; Morokuma, K. *J. Am. Chem. Soc.* **1992**, *114*, 2359.
(27) Kawamura-Kuribayashi, H.; Koga, N.; Morokuma, K. *J. Am. Chem. Soc.* **1992**, *114*, 8687.
(28) Bierwagen, E. B.; Bercaw, J. E.; Goddard, W. A., III *J. Am. Chem. Soc.* **1994**, *116*, 1481.
(29) Gleiter, R.; Hyla-Kryspin, I.; Niu, S.; Erker, G. *Organometallics* **1993**, *12*, 3828.
(30) Mohr, R.; Berke, H.; Erker, G. *Helv. Chim. Acta* **1993**, *76*, 1389.
(31) Froese, R. D. J.; Musaev, D. G.; Matsubara, T.; Morokuma, K. *J. Am. Chem. Soc.* **1997**, *119*, 7190.
(32) Weiss, H.; Ehrig, C.; Ahlrichs, R. *J. Am. Chem. Soc.* **1994**, *116*, 4919.
(33) Yoshida, T.; Koga, N.; Morokuma, K. *Organometallics* **1995**, *14*, 746.
(34) Margl, P.; Deng, L.; Ziegler, T. *Organometallics* **1998**, *17*, 933−946.
(35) Woo, T.; Margl, P. M.; Lohrenz, J. C. W.; Blöchl, P. E.; Ziegler, T. *J. Am. Chem. Soc.* **1996**, *118*, 13021.
(36) Woo, T. K.; Margl, P.; Ziegler, T.; Blöchl, P. E. *Organometallics* **1997**, *16*, 3454.
(37) Baerends, E. J.; Ellis, D. E.; Ros, P. *Chem. Phys.* **1973**, *2*, 41.
(38) Baerends, E. J.; Ros, P. *Chem. Phys.* **1973**, *2*, 52.
(39) Ravenek, W. In *Algorithms and Applications on Vector and Parallel Computers*; te Riele, H. J. J., Dekker, T. J., van de Horst, H. A., Eds.; Elsevier: Amsterdam, The Netherlands, 1987.
(40) te Velde, G.; Baerends, E. J. *J. Comput. Chem.* **1992**, *99*, 84.
(41) Boerrigter, P. M.; te Velde, G.; Baerends, E. J. *Int. J. Quantum Chem.* **1988**, *33*, 87.
(42) Versluis, L.; Ziegler, T. *J. Chem. Phys.* **1988**, *88*, 322.
(43) Snijders, J. G.; Baerends, E. J.; Vernoijs, P. *At. Nucl. Data Tables* **1982**, *26*, 483.
(44) Vernoijs, P.; Snijders, J. G.; Baerends, E. J. *Slater Type Basis Functions for the Whole Periodic System*; Internal report (in Dutch); Department of Theoretical Chemistry, Free University: Amsterdam, The Netherlands, 1981.
(45) Krijn, J.; Baerends, E. J. *Fit Functions in the HFS Method*; Internal Report (in Dutch); Department of Theoretical Chemistry, Free University: Amsterdam, The Netherlands, 1984.
(46) Vosko, S. H.; Wilk, L.; Nusair, M. *Can. J. Phys.* **1980**, *58*, 1200.
(47) Becke, A. *Phys. Rev. A* **1988**, *38*, 3098.

corrections and Perdew's[48,49] nonlocal correlation correction. Geometries were optimized including nonlocal corrections. First-order scalar relativistic corrections[50,51] were added to the total energy for all systems containing 3d and 4d metal atoms, since a perturbative relativistic approach is sufficient for those as shown by Deng et al.[52] On all systems containing lanthanide, actinide, or 5d metal atoms, quasirelativistic calculations were carried out.[53] In view of the fact that all systems investigated in this work show a large HOMO−LUMO gap, a spin restricted formalism was used in all calculations for $d^0$ systems and for the $d^2$ system ([1]$NbC_2H_5$). For [2]Ti(III)$C_2H_5$ (a $d^1$ complex), a spin-unrestricted formalism was used. The role of spin multiplicity for systems with non-$d^0$ occupations is currently under investigation[54] and is supposed to markedly influence barrier heights. No symmetry constraints were used except where explicitly indicated. Transition states were located by keeping a specific internal coordinate (the reaction coordinate) fixed in a linear-transit fashion while optimizing all other degrees of freedom. The internal coordinate in this case was the distance between the carbon atoms of the new bond that is formed during insertion. These calculations were assumed to be converged if the force on the reaction coordinate was smaller than 0.002 hartree/bohr. No frequencies were calculated to characterize the obtained transition state. For the ethylene insertion reaction this criterion gives activation energies converged to within less than 1 kJ/mol. In a number of previous papers where the same level of theory was used, transition metal−ligand dissociation energetics have been proven to be correct within 20 kJ/mol of the experimental result,[55−58] usually overestimated in terms of absolute size. Activation energies have been shown to be generally lower by 8−16 kJ/mol than the experimental estimate.[59,60] Neither zero-point nor finite-temperature corrections were added to the energies reported here due to the high expense of calculating second derivatives of the total energy with respect to the nuclei. A discussion of zero-point and finite-temperature corrections for the example of $Cp_2ZrC_2H_5(C_2H_4)^+$ has been provided by Lohrenz et al.[61]

## Results and Discussions

**(a) Geometries and Energetics of the Ethylene Insertion Transition States [L]M··$C_2H_4$··$C_2H_5^{n+}$ ($n$ = 0, 1, 2).** In the following, we describe in detail the factors responsible for the systematic trends in the calculated activation barriers for ethylene insertion. Geometries of all ethylene insertion transition states mentioned in this work are given in the Supporting Information.

For all subsequent deliberations it is useful to consider a [L]M fragment with $C_{2v}$ pseudosymmetry. Scheme 3 shows a typical arrangement of ligands where two coordination sites are occupied by the auxiliary ligand set [L]. The growing chain (in this case ethyl) occupies the remaining coordination sites with the M−$C_\alpha$ bond and typically one or two agostic bonds,[34−36,61,62] where C−H linkages are bound to the metal center through hydrogen. The $\beta$-agostic bond involving hydrogens on the $\beta$-carbon is usually strongest.[61] If more than two coordination sites are occupied by an auxiliary ligand, agostic interactions decrease in strength due to steric congestion.

**Scheme 3**

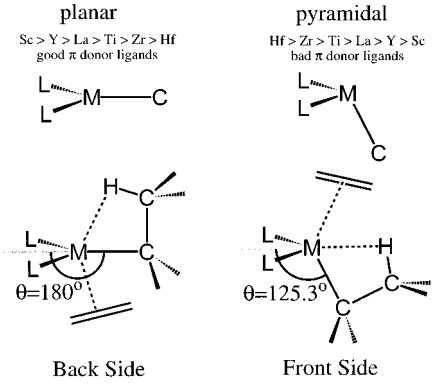


**Scheme 4**

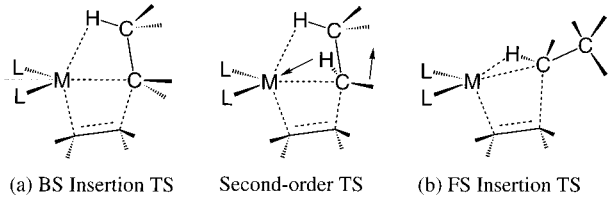


In previous work, it was observed that an incoming olefin forms a $\pi$-complex prior to insertion.[34−36,61,62] Complex formation can occur syn or anti to an already existing $\beta$-agostic bond. We will retain the convention of terming the resulting complexes the frontside (FS) and backside (BS) complex, respectively (Scheme 2).

The relative preferences of FS and BS $\pi$-complexation have been outlined in the first part of this study[34] and by Bierwagen et al.[28] It was found there that ethylene uptake energetics are dominated by the total charge on the complex and the openness of the active site, as measured by the accessible surface area on the metal ion. The conformation of the $\pi$-complex (BS vs FS) was influenced by the nature of the metal and the auxiliary ligand. The propensity to form a FS complex increases from 3d to 5d metals and from group 3 to group 4 metals (Scheme 3). Good $\pi$-donor ligands such as amido groups were found to stabilize the BS complex. The sole origin of this behavior was the deformability of the [L]M$C_2H_5^{n+}$ framework, which increasingly prefers a pyramidal arrangement of ligands over a planar arrangement as one goes down a triad and from group 3 to group 4 metals. FS and BS $\pi$-complexation give rise to different insertion pathways as the incoming olefin can approach the M−$C_\alpha$ bond from two sides. Correspondingly, those insertions will be termed FS and BS insertion, respectively.

The olefin insertion reaction is generally believed to proceed through a four-centered transition state such as shown in Scheme 4.[31−33,35,61,63−65] Agostic interactions have been shown by numerous theoretical investigations to be vital throughout the insertion process since they provide stabilization for the carbon network during the bond rearrangement process.[22,25−27,29−33,35,61] It has been observed previously that attack originating from a BS position often leads to an insertion transition state (TS) that has a strong $\beta$-agostic interaction (Scheme 4a) and that attack starting from a FS $\pi$-complex predominantly results in a TS that is predominantly stabilized by an α-agostic bond[35,61] (Scheme 4b).

Higher-order agostic bonds (such as $\gamma$ and $\delta$) have been observed[35,61] to dissociate upon $\pi$-complex formation and hence do not figure in the insertion TS. Let us now for the purpose of the following discussion define the activation barrier for insertion $\Delta E^{\ddagger}_{ins}$ (eq 1) as the difference of the total energies of

(48) Perdew, J. P. *Phys. Rev. B* **1986**, *34*, 7406.
(49) Perdew, J. P. *Phys. Rev. B* **1986**, *33*, 8822.
(50) Snijders, J. G.; Baerends, E. J. *Mol. Phys.* **1978**, *36*, 1789.
(51) Snijders, J. G.; Baerends, E. J.; Ros, P. *Mol. Phys.* **1979**, *38*, 1909.
(52) Deng, L.; Ziegler, T.; Woo, T. K.; Margl, P.; Fan, L. *Organometallics.* **1998**. In press.
(53) Ziegler, T.; Tschinke, V.; Baerends, E. J.; Snijders, J. G.; Ravenek, W. *J. Phys. Chem.* **1989**, *93*, 3050.
(54) Schmid, R.; Ziegler, T. Work in progress.
(55) Folga, E.; Ziegler, T. *J. Am. Chem. Soc.* **1993**, *115*, 5169.
(56) Li, J.; Schreckenbach, G.; Ziegler, T. *J. Phys. Chem.* **1994**, *98*, 4838.
(57) Li, J.; Schreckenbach, G.; Ziegler, T. *J. Am. Chem. Soc.* **1995**, *117*, 486.
(58) Li, J.; Schreckenbach, G.; Ziegler, T. *Inorg. Chem.* **1995**, *34*, 3245.
(59) Margl, P. M.; Ziegler, T. *J. Am. Chem. Soc.* **1996**, *118*, 7337.
(60) Margl, P.; Ziegler, T. *Organometallics* **1996**, *15*, 5519.
(61) Lohrenz, J. C. W.; Woo, T. K.; Ziegler, T. *J. Am. Chem. Soc.* **1995**, *117*, 12793.

the insertion transition state ($E^{\ddagger}$) and the $\pi$-complex ($E$)

$$\Delta E^{\ddagger}_{\mathrm{ins,FS}} = E^{\ddagger}_{\mathrm{FS}} - E_{\mathrm{FS}} \text{ and } \Delta E^{\ddagger}_{\mathrm{ins,BS}} = E^{\ddagger}_{\mathrm{BS}} - E_{\mathrm{BS}} \quad (1)$$

Here, the indices FS and BS serve to distinguish between FS and BS insertion pathways.

**(b) Trends of the Olefin Insertion Barriers.** From Table 1 and Figure 1 it is apparent that ethylene insertion barriers are rather low and tend to be lower for light metals than for heavy metals. Lauher and Hoffmann[66] have recognized very early that for $d^0$ systems such as $Cp_2Ti(C_2H_4)H^+$, the absence of a barrier for insertion of olefin into the M−H bond can be rationalized within a simple three-orbital-four-electron picture. Their rationale was that in $d^0$ systems, the LUMO would consist mainly of a bonding ethylene $\pi^*$−metal d contribution, which is shifted upward as the insertion approaches the transition state. Since the LUMO does not contribute to the total energy, insertions in $d^0$ complexes were predicted to be barrierless, whereas insertions in $d^2$ complexes should have a substantial barrier.

Our nonlocal DFT calculations show a similar picture, with three orbitals and two electron pairs effectively taking part in the reaction. Figure 2 shows a MO diagram highlighting the major changes of the energy levels as the reaction proceeds. In the $\pi$-complex, the LUMO is predominantly made up of a bonding metal d−olefin $\pi^*$ contribution. The $C_\alpha$ $sp^3$ orbital as well as the ethylene $\pi$ orbital are lower in energy and occupied with 2 electrons each. In the transition state, the occupied ethyl $sp^3$ lobe and the occupied olefin $\pi$ orbital form a bonding and an antibonding combination, thus giving rise to an energetically unfavorable two-orbital-four-electron interaction. To relieve the electron pair in the antibonding orbital, the higher-lying—but empty—olefin $\pi^*$ orbital mixes in, creating essentially an olefin−ethyl nonbonding HOMO. Conversely, this $\pi-\pi^*$ mixing serves to increase the energy of the LUMO by enforcing its ethyl−olefin antibonding character. In the case of $d^0$ complexes, it becomes obvious that insertion of olefin into the M−ethyl bond will be barrierless, whereas $d^2$ complexes should not undergo insertion in this fashion.

To fortify this point, we have calculated the barrier for the process [1]Nb(III)$C_2H_5 + C_2H_4 \rightarrow$ [1]Nb(III)(butyl). The olefin uptake energy for this $d^2$ system is much larger than that for $d^0$ metals (−207 kJ/mol) due to the donation of high-lying metal d electrons into the lower-lying olefin $\pi^*$ orbital.[34] Also, the barrier for insertion is 196 kJ/mol (Table 1), which is approximately 10 times higher than for the analogous Sc(III) $d^0$ complex, making olefin insertion virtually impossible. The orbital picture as discussed above is retained in this case, with the doubly occupied ethyl−ethylene antibonding orbital residing in the HOMO. Similarly, adding an extra electron to [7]Ti$C_2H_5$-$(C_2H_4)^+$ (giving [7]Ti$C_2H_5(C_2H_4)$) results in an olefin insertion barrier of 92 kJ/mol, again substantially higher than the ≈20 kJ/mol observed for the $d^0$ parent complex (see also Figure 1). From this, one can conclude that $d^1$ and $d^2$ complexes will generally not be good olefin insertion catalysts, unless the offending d electrons can be donated into a ligand orbital orthogonal to the ethylene $\pi^*$ orbital. An example of this has

**Table 1.** Ethylene Insertion Barriers for All Compounds Investigated

| | | TS energy[a] | | direct insertion barrier[b] | | reaction coordinate at TS[c] | |
|---|---|---|---|---|---|---|---|
| metal | ligand | FS | BS | FS | BS | FS | BS |
| Sc[III] | [1]-exo | −24 | −32 | 6 | 13 | 2.2 | 2.18 |
| | [2]-exo | −33 | −35 | 20 | 10 | 2.3 | 2.1 |
| | [3][e] | −56 | | 27 | 4 | 2.5 | |
| | [4] | 6 | 28 | 6 | 33 | 3.9 | 2.1 |
| | [7][e] | −27 | | 11 | 20 | 2.2 | |
| | [8] | −29 | −31 | 17 | 15 | 2.25 | 2.18 |
| | [9] | −35 | −26 | 11 | 15 | 2.3 | 2.08 |
| Y[III] | [1]-exo[d] | −30 | −34 | 16 | 18 | 2.2 | 2.15 |
| | [7][e] | −27 | | 23 | 21 | 2.2 | |
| | [8][e] | −27 | | 26 | 16 | 2.19 | |
| | [9][e] | −29 | | 26 | 11 | 2.25 | |
| La[III] | [1]-exo[d] | −14 | −16 | 24 | 26 | 2.2 | 2.14 |
| | [7][e] | −7 | | 29 | 17 | 2.17 | |
| | [8][e] | −10 | | 28 | 11 | 2.22 | |
| | [9][e] | −2 | | 38 | 16 | 2.2 | |
| Lu[III] | [1]-exo[j] | −29 | −34 | 29 | | 2.4 | 2.4 |
| Ti[III] | [7][e,k] | −12 | | 92 | 92 | 2.02 | |
| Nb[III] | [1]-exo[k,l] | | −11 | | 196 | | 2.04 |
| Ti[IV] | [1]-exo | −75 | −89 | 13 | 0 | 2.18 | 2.3 |
| | [1]-endo | −90 | −61 | 0 | 21 | 2.2 | 2.07 |
| | [2]-exo | −62 | −75 | 28 | 0 | 2.25 | 2.1 |
| | [2]-endo | −94 | −63 | 3 | 19 | 2.3 | 2.1 |
| | [3][e] | −128 | | 33 | 33 | 2.5 | |
| | [4] | 7 | 8 | 15 | 21 | 3.8 | 2.1 |
| | [5][h] | −64 | −55 | 20 | 22 | 2.41 | 2.11 |
| | [7] | −78 | −80 | 18 | 20 | 2.25 | 2.13 |
| | [8] | −75 | −87 | 34 | 7 | 2.77 | 2.27 |
| | [9][e] | −79 | | 23 | 4 | 2.28 | |
| | [10]-exo[f,g,m] | −49 | −47 | 13 | 33 | 2.08 | 2.14 |
| | [10]-endo[f,g,m] | −47 | −49 | 24 | 29 | 2.14 | 2.08 |
| | [11]-exo[m,n] | −58 | −66 | 36 | 8 | 2.5 | 2.23 |
| Zr[IV] | [1]-exo[d] | −70 | −83 | 27 | 3 | 2.2 | 2.2 |
| | [3][e] | −125 | | 40 | 40 | 2.35 | |
| | [4][i] | −23 | −27 | 17 (22) | 28 | 2.299 | 2.02 |
| | [7] | −72 | −73 | 32 | 24 | 2.22 | 2.08 |
| | [8][e] | −73 | | 36 | 13 | 2.22 | |
| | [9][e] | −78 | | 34 | 5 | 2.3 | |
| | [10]-exo[f,g,m] | −62 | −62 | 24 | 30 | 2.089 | 2.072 |
| | [10]-endo[f,g,m] | −62 | −62 | 24 | 27 | 2.072 | 2.089 |
| | [11]-exo[m,n] | −51 | −63 | 54 | 13 | 2.32 | 2.20 |
| Hf[IV] | [1]-exo[d] | −55 | −64 | 46 | 38 | 2.493 | 2.38 |
| | [4] | −45 | −36 | 18 | 27 | 2.3 | 2.085 |
| | [7][j] | −33 | −38 | 54 | | 2.5 | 2.2 |
| | [8][j] | −30 | −44 | 71 | | 2.7 | 2.35 |
| | [9][e,j] | −22 | | 64 | | 2.36 | |
| | [10]-exo[f,g,m] | −49 | −49 | 36 | 40 | 2.198 | 2.179 |
| | [10]-endo[f,g,m] | −49 | −49 | 40 | 28 | 2.179 | 2.198 |
| Ce(IV) | [1]-exo[d] | −28 | −30 | 34 | 19 | 2.3 | 2.23 |
| Th(IV) | [1]-exo[j] | −34 | −34 | 40 | | 2.3 | 2.2 |
| V(V) | [6] | −9 | −25 | 5 | 4 | 2.2 | 2.25 |

[a] In kJ/mol. Relative to the most stable conformation of the precursor [L]M$C_2H_5^{n+}$ + free $C_2H_4$. [b] In kJ/mol. Relative to the $\pi$-complex [L]M$C_2H_5(C_2H_4)^{n+}$. FS barriers relative to the FS $\pi$-complex, BS barriers relative to the BS $\pi$-complex. Exo(endo) barriers relative to exo(endo) conformation of the $\pi$-complex. [c] In angstrom units. The reaction coordinate is defined as the distance between carbon atoms between which the bond is formed. [d] For some compounds of the type [1]M$C_2H_5^{n+}$, BS(exo) and FS(endo) complexes are geometrically and energetically very similar. Due to the flatness of the potential surface with regard to this interconversion, the FS(endo) and BS(exo) pathways are no longer well-defined. The BS(exo) insertion barrier should therefore be interpreted with caution. [e] FS and BS transition states are identical. [f] Results taken from Deng et al.[52] [g] BS(exo) and FS(endo) transition states are identical. [h] Results taken from Woo et al.,[35] who used nonlocal perturbation energetics on geometries obtained with LDA. [i] Results taken from Lohrenz et al.,[61] who used nonlocal perturbation energetics on geometries obtained with LDA. Note that there, the total FS insertion barrier was decomposed into a part corresponding to rotation of the ethyl ($\Delta E^{\ddagger}$ = 14 kJ/mol) and one corresponding to insertion ($\Delta E^{\ddagger}$ = 2.5 kJ/mol). The value in parentheses corresponds to a fully nonlocal calculation. The RC value of 2.299 Å was measured at the top of the insertion energy profile. Geometries in ref 61 were optimized with constrained Cp rings. [j] Does not form a stable BS $\pi$-complex, so no direct BS activation barrier can be given. [k] Not a $d^0$ system. [l] FS attack leads to C−H activation. [m] Propyl group used to model the growing polymer chain. [n] The corresponding $\pi$-complexation energies (not listed in part 1 of this study) are as follows: [11]Ti$C_3H_7$+(exo) (FS: −94 kJ/mol; BS: −74 kJ/mol); [11]Zr$C_3H_7$+(exo) (FS: −105 kJ/mol; BS: −77 kJ/mol).

(62) Margl, P.; Lohrenz, J. C. W.; Ziegler, T.; Blöchl, P. E. *J. Am. Chem. Soc.* **1996**, *118*, 4434.
(63) Siegbahn, P. E. M. *Chem. Phys. Lett.* **1993**, *205*, 290.
(64) Meier, R. J.; vanDormaele, G. H. J.; Iarlori, S.; Buda, F. *J. Am. Chem. Soc.* **1994**, *116*, 7274.
(65) Fan, L.; Harrison, D.; Woo, T. K.; Ziegler, T. *Organometallics* **1995**, *14*, 2018.
(66) Lauher, J. W.; Hoffmann, R. *J. Am. Chem. Soc.* **1976**, *98*, 1729.

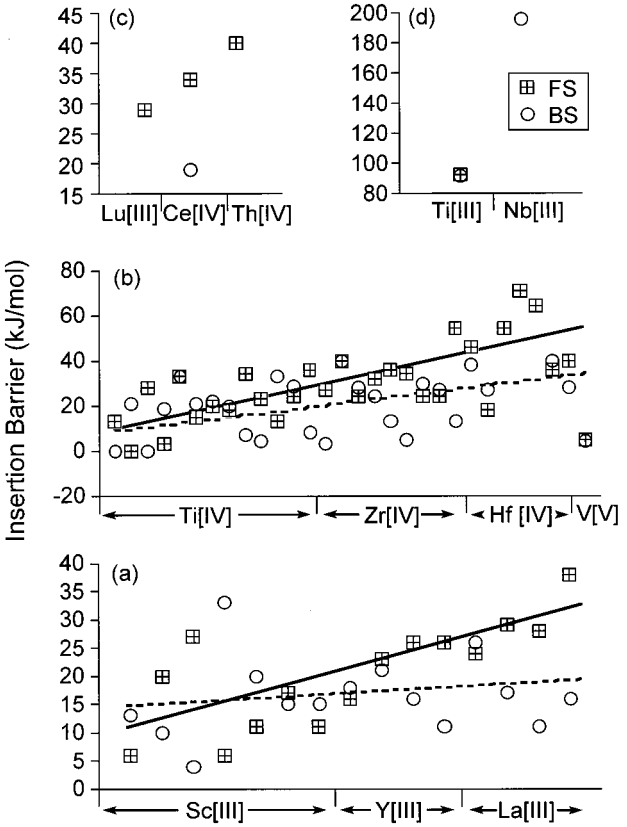


**Figure 1.** Barriers for the insertion of ethylene (*y* axis) into the M−$C_\alpha$ bond of various $d^0$ catalyst systems (*x*-axis) in units of kJ/mol. Systems are grouped on the *x*-axis according to the central metal atom, with data points in the same sequence as they appear in Table 1. Circles refer to the BS insertion barrier and squares to the FS insertion barrier. Lines refer to linear fits through insertion barriers for the Sc (a) and Ti (b) triad. To make the fit independent of the sequence in which the ligands appear, each fit was formulated with respect to the average over all FS(BS) insertion barriers for a given metal. Full lines correspond to FS insertion barriers. Dashed lines correspond to BS insertion barriers. Barriers for compounds of (a) the Sc triad, (b) the Ti triad and V, (c) lanthanides and actinides, and (d) $d^1$ and $d^2$ systems. Note the high activation barriers for the non-$d^0$ systems with Ti[III] and Nb[III] centers. The linear fit through the BS insertion barriers for the Ti triad (b, dashed line) shows an artificially enhanced slope since there are no BS insertion data points for $[L]HfC_2H_5^+$ (L = 7, 8, 9). If one was to measure a BS insertion barrier from the top of the negatively curved BS $\pi$-complex plateau for these compounds, the slope of the BS fit in (b) would drop significantly.

been given experimentally by Nakamura et al.,[67] who reported living olefin polymerization with complexes of the type M($\eta^5$-$C_5Me_5$)($\eta^4$-diene)$X_2$ (M = Nb(III), Ta(III)). In this case, the d electron pair can be donated into the empty diene $\pi$* orbital and therefore does not occupy the olefin−polymer antibonding interaction. In cases where there is no ligand orbital to accept the extra d electrons, the barrier will also be low if the metal d-orbitals are lower in energy than the emerging olefin−polymer antibonding interaction (e.g., for late transition metals) or cannot be donated into the olefin $\pi$* orbital due to symmetry reasons. An alternative way of stating the same fact is to say that the energetic stabilization gained from donation of two electrons into the olefin $\pi$* orbital must be given up since there is no analogous empty ligand orbital to receive these electrons in the product state.

(67) Mashima, K.; Fujikawa, S.; Tanaka, Y.; Urata, H.; Oshiki, T.; Tanaka, E.; Nakamura, A. *Organometallics* **1995**, *14*, 2633.

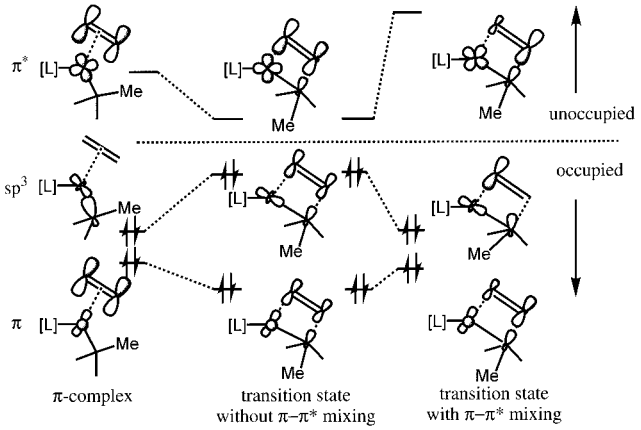


**Figure 2.** Molecular orbital diagram of the mixing process involved in the insertion of olefin into a metal−carbon bond, abstracted from DFT calculations for several $d^0$ complexes. A full MO plot for this reaction is given in the supporting material. Orbital occupations are shown for the formal $d^0$ configuration of the metal. Note that although the metal has formally no d electrons, there is some d orbital character present in the bonding orbitals. The exact shape and composition of the d contributions to individual orbitals varies between systems.

We can conclude this section by stating that in general, $d^0$ and $d^0f^n$ transition metal alkyl complexes intrinsically have a low barrier for ethylene insertion into the M−$C_a$ bond due to the absence of an alkyl−olefin antibonding interaction. A high barrier can be expected for transition metal complexes which have a nonzero d electron count and whose d electrons have the appropriate energy and symmetry to be donated into the emerging olefin−polymer antibonding MO. Therefore, late transition metals, which have lower d orbital energies, will not exhibit significantly higher olefin insertion barriers even if they have a nonzero d electron count, whereas early transition metals with high d electron energies will exhibit a substantial barrier if d electrons are present at the metal. Our calculations make it clear that the reason some $d^0$ catalyst systems do perform well under experimental conditions and some do not is clearly not related to the height of the insertion barrier, but must be related to other factors such as competing termination reactions. Such termination reactions and how they affect catalyst performance will be investigated in the sequel to this paper.[68] Although insertion barriers for $d^0$ systems are low, they *do* show dependence upon both ligand and metal. The issue of how the insertion barrier can be tuned will be discussed next.

**(c) Tuning the Insertion Barrier of Systems without Steric Encumbrance ($[L]MC_2H_5^{n+}$; L = 7, 8, 9).** From Figure 1 we can see that among $d^0$ systems, there is a rising trend for the FS insertion barrier as one goes down the triad and from group 3 to group 4 metals, irrespective of the ligand that is used. To study these systematic variations of olefin insertion barriers, we carried out a series of calculations on systems of the general composition $L_2MC_2H_5^{n+}$ (M = Sc(III), Y(III), La(III), Ti(IV), Zr(IV), Hf(IV); L = $CH_3$, $NH_2$, OH). The two ligand groups L are kept at a typical bidentate angle of 90° to each other by means of a constraint but are otherwise free to change. This makes it possible to study the systematic change of the insertion barrier in the absence of steric encumbrance and under pseudo-$C_{2v}$ symmetric conditions.

**(c.1) Tuning the Olefin Insertion Barrier by Changing the Metal.** Figure 3 shows that direct FS insertion barriers increase as one goes down a triad and from group 3 to group 4 metal centers. This increase is more profound for group 4 cations

(68) Margl, P.; Ziegler, T. **1997**, manuscript in preparation.

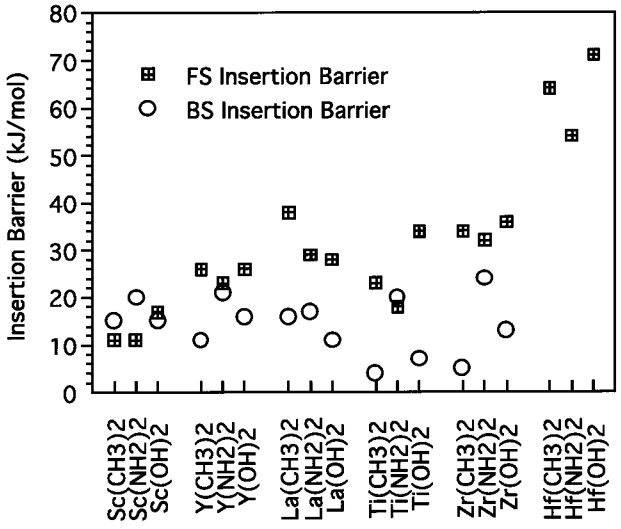


**Figure 3.** Insertion barriers for sterically minimal ligand systems in kJ/mol. Barriers are measured from FS $\pi$-complex to FS transition state and from BS $\pi$-complex to BS transition state. For [L]$HfC_2H_5^+$, the BS $\pi$-complex is unstable, therefore the BS insertion barrier is omitted.

than for group 3 metals. We can understand these trends by decomposing[69] the insertion barriers for complexes of the type $(NH_2)_2MC_2H_5(C_2H_4)^{n+}$ (M = Sc(III), Y(III), La(III), Ti(IV), Zr(IV), Hf(IV)) according to eq 2, as shown in Table 2.

For a discussion of barrier heights it is convenient to decompose the activation barrier for ethylene insertion according to eq 2

$$\begin{aligned}\Delta E^{\ddagger}_{\text{ins}} &= \Delta E_{\text{detach}} + \Delta E_{\text{def,}C_2H_4} + \Delta E_{\text{def,[L]}MC_2H_5} + \Delta E_{\text{attach}} \\ &= \Delta E_{\text{detach}} + \Delta E_{\text{def}} + \Delta E_{\text{attach}} \\ &= \Delta E_{\pi} + \Delta E_{\text{def}} \end{aligned} \quad (2)$$

and Scheme 5. This decomposition isolates the two important contributions to the barrier which arise (a) from the binding of the ethylene to the [L]$MC_2H_5^{n+}$ fragment ($\Delta E_{\text{detach}} + \Delta E_{\text{attach}} = \Delta E_{\pi}$) and (b) from the deformation of the ethylene ($\Delta E_{\text{def,}C_2H_4}$) and [L]$MC_2H_5^{n+}$ ($\Delta E_{\text{def,[L]}MC_2H_5}$) fragments.

The strongest trend observable in Table 2 and Figure 3 is certainly the increase of the FS insertion barrier as one goes down a triad. Table 2 shows this behavior to be predominantly caused by the increasing deformation energy of the metal fragment $(NH_2)_2MC_2H_5^{n+}$, which outweighs all other factors. It is important to note that the deformation angle $\theta_{\text{ins}}$ (for a definition of $\theta$ see Scheme 3) is very similar ($\approx$150°) for all insertion transition state structures, regardless of the metal. That means that the metal framework geometry is practically identical for all FS transition states. Therefore, one can correlate the barrier height for FS insertion with the energy that is necessary to deform the metal framework into the TS geometry. In part one of this study we have shown that the propensity to form a planar metal−ligand framework is stronger for light metals than for heavy metals and stronger for group 3 metals than for group 4 metals. The formation of a FS transition state from a FS $\pi$-complex is a process that shifts the metal−ligand framework toward planar coordination since the ethylene and the polymer chain terminus approach each other to meet opposite the auxiliary ligands. Therefore, the stronger the propensity of the precursor complex [L]$MC_2H_5^{n+}$ to form a planar metal−ligand framework, the lower the barrier of FS insertion. Group 3 metal complexes show lower FS insertion barriers than group 4 metal complexes. As one moves down a triad, the FS insertion barrier increases.

For sterically unhindered systems, FS and BS insertion pathways lead through the same transition state geometry (with few exceptions, see Table 1) since alkyl rotation is facile (Scheme 4), so that FS TS and BS TS as well as the second-order TS that connects them collapse to one point. In cases where FS- and BS-TS are not exactly identical, they are energetically very close (largest difference $E_{\text{BSTS}} - E_{\text{FSTS}} =$ 14 kJ/mol for [8]$HfC_2H_5(C_2H_4)^+$). In such cases, the relative heights of FS and BS insertion barriers are determined by the energies of the $\pi$-complexes. The BS insertion barrier is generally smaller than the FS insertion barrier as the BS $\pi$-complex is usually disfavored compared to the FS $\pi$-complex for electronic reasons.[34] BS insertion barriers exhibit only a minor metal influence since they require no deformation of the metal−ligand framework.

**(c.2) Tuning the Olefin Insertion Barrier by Varying the Auxiliary Ligand.** Figure 3 also shows a remarkable alternating pattern of insertion barriers with respect to the auxiliary ligands. Amido-complexed systems tend to have a lower FS insertion barrier but a higher BS insertion barrier than the hydroxy or the methyl systems and vice versa. We note that such an equivalent pattern has already been observed for ethylene complexation energies in Part 1 of this study[34] where it was shown to originate from different deformabilities of the $L_2MC_2H_5^{n+}$ precursor complexes. It was concluded that a high propensity to form a planar arrangement of ligands enhances BS $\pi$-complexation whereas an aptitude to form a pyramidal metal−ligand framework enhances FS $\pi$-complexation. It was shown that good $\pi$-donor ligands such as $NH_2$ enforce planar configuration and thus BS complexation. In such cases, the BS $\pi$-complex is low in energy compared to the FS $\pi$-complex. To understand the variations of the direct insertion barriers with respect to the auxiliary ligand set, we again have to appreciate the fact that FS and BS transition states are identical (geometrically as well as energetically) for most metal−ligand combinations shown in Table 1. For sterically minimal ligands (and in general for bidentate ligands which have little steric bulk), the relative heights of FS and BS insertion barriers are mostly determined by the relative energy of FS and BS $\pi$-complexes. Since a strongly stabilized FS complex is concomitant with a strongly destabilized BS complex, a high FS insertion barrier goes hand in hand with a low BS insertion barrier and vice versa.

**(c.3) Insertion Kinetics for Ligands without Steric Bulk (L = 7, 8, 9).** We have found that for sterically rigid bidentate systems with $C_{2v}$ symmetry the general picture for the insertion reaction looks as follows: FS and BS insertion transition states are identical (or nearly so) in terms of both geometry and total energy. Steady-state kinetics dictate that in such a case, BS and FS pathways will experience the same reactive flux,[71] regardless of the interconversion barrier between BS and FS $\pi$ complexes. However, the activity of the catalyst is restrained by the higher one of the two activation barriers, which for sterically minimal ligands is usually the FS barrier due to the better energetic stabilization of the FS $\pi$ complex. It follows that the rate-limiting step for most sterically minimal, rigid $C_{2v}$ symmetric catalysts is the FS barrier. This, in turn, is determined by the flexibility of the metal−ligand framework which is high for light transition metals and group 3 transition metals.

(69) Ziegler, T.; Rauk, A. *Theor. Chim. Acta* **1977**, *46*, 1.

**Table 2.** Decomposition of the Ethylene FS Insertion Barrier into the M−$C_\alpha$ Bond of $(NH_2)_2MC_2H_5^{n+}$ [a]

| | $\Delta E_{detach}$ | $\Delta E_{Def}$ | | $\Delta E_{attach}$ | $\Delta E_\pi$ | $\Delta E_{Def}$ | $\Delta E_{rel}$ | $\Delta E^{\ddagger}_{ins}$ [b] | $\theta_{ins}$ [c] |
|---|---|---|---|---|---|---|---|---|---|
| | | $C_2H_4$ | $[L]MC_2H_5^{n+}$ | | | | | | |
| Sc | 52 | 37 | 20 | −99 | −47 | 57 | 0 | 10 | 148 |
| Y | 51 | 43 | 29 | −102 | −51 | 72 | 1 | 22 | 149 |
| La | 38 | 47 | 37 | −94 | −56 | 84 | (0) | 29 | 152 |
| Ti | 103 | 32 | 46 | −163 | −60 | 78 | 0 | 18 | 154 |
| Zr | 102 | 43 | 55 | −169 | −67 | 98 | 0 | 32 | 152 |
| Hf | 98 | 19 | 92 | −155 | −57 | 111 | (0) | 54 | 156 |

[a] Energies in kJ/mol. Values in parentheses are relativistic corrections which are already contained in $\Delta E_\pi$ and $\Delta E_{def}$. [b] Individual contributions might not exactly add up to $\Delta E^{\ddagger}_{ins}$ due to roundoff errors. [c] $\theta_{ins}$ refers to the angle between the N−N centroid, the M atom, and the $C_\alpha$ atom, measured at the FS transition state geometry.

**Scheme 5**

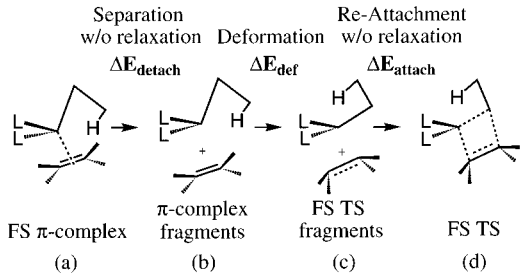


We conclude that the activity of a catalyst ligated by a sterically undemanding bidentate ligand of approximate $C_{2v}$ symmetry—as judged solely by the rate of insertion—decreases as one moves down the triad and from group 3 metals to group 4 metals.

The data presented in Sections c.1 to c.3 can be used to custom-design catalysts by simply varying the metal and/or the ligand environment. A given catalyst $[L]MR^+$ can be made more active by substituting a heavy metal with a light one or by going from a group 4 metal to a group 3 one. If a given metal center is specified, switching from a weak $\pi$-donor such as an oxygen ligand to a good $\pi$-donor such as an amido group will serve to enhance catalyst activity. One should, however, bear in mind that these rules only pertain to the *intrinsic* activity of a catalyst and do not account for influences that are not directly related to the insertion barrier, such as catalyst blocking by a counterion or steric effects. We will in the following section show how steric effects can be employed as useful tools to override the intrinsic preferences outlined in Section c.

**(d) Modifying the Olefin Insertion Barrier by Steric Bulk—Realistic Ligands.** Steric factors are expected to modify the potential energy surface for olefin insertion. As the olefin approaches the metal−$C_\alpha$ bond from the front side, the $\beta$-agostic interaction that supports the chain in the precursor and $\pi$-complex phases must give way to allow the formation of a bond between olefin and alkyl α-carbon. This process usually takes place by rotation of the alkyl chain around the M−$C_\alpha$ bond. If the steric constriction around the metal center is such that it does not allow the $\beta$-agostic bond to be maintained during this process, some bond rupture barrier will be observed[61] as opposed to a case where the $\beta$-agostic bond can be maintained throughout the FS insertion process. For the BS insertion process, the dependence of the insertion barrier upon steric bulk will be comparatively smaller, since the $\beta$-agostic bond can be maintained throughout the reaction.

**(d.1) Sterically Undemanding, $C_{2v}$ Symmetric Auxiliary Ligands.** The results we obtain for the *acac*-type ligand [3] as shown in Table 1 confirm that the conclusions drawn from sterically minimal ligands hold well for realistic systems if the additional steric bulk is small enough. For $[3]ScC_2H_5^+$, $[3]TiC_2H_5^{2+}$, and $[3]ZrC_2H_5^{2+}$, FS and BS insertion TS are identical—a fact that one would expect by extrapolating from our data obtained for minimal ligands [7], [8], and [9]. Also, direct as well as indirect insertion barriers increase from group 3 to group 4 as well as from Ti to Zr, a trend that was already pointed out from minimal ligands. Although the insertion barriers for complexes of [3] are slightly higher than those for [7], [8], and [9] owing to the stronger stabilization of the $\pi$-complex by an enhanced electrostatic interaction, the overall trends confirm our calculations on "artificial"—sterically minimal—systems. This confirms our previous assumption that sterically minimal systems are a valid substitute for realistic systems if the systems to be modeled do not infringe on the openness of the active site.

**(d.2) Sterically Constricted, Pseudo-$C_{2v}$ Symmetric Auxiliary Ligands.** The most popular example for a sterically demanding, pseudo-$C_{2v}$ symmetric ligand is the bis-Cp system [4]. It acts to restrain the angular freedom of the alkyl chain as expressed by the deformation angle $\theta$ and also restrains the rotation of the alkyl around the M−$C_\alpha$ bond. Therefore, one would expect the geometries for FS and BS $\pi$-complexation to be very different since the rotation that interconverts these is sterically blocked. Indeed, we find this to be the case for all systems of ligand [4] investigated here (Table 1), as shown by the radically different value of the reaction coordinate. Generally, the FS insertion transition state is early as measured by the reaction coordinate (RC) (RC ≈ 4 (Sc, Ti) to 2.3 Å (Hf)), whereas the BS TS is late (RC ≈ 2.1 to 2.0 Å). This is due to the fact that the steric constriction around the metal does not allow the $\beta$-agostic bond to be maintained throughout the FS approach of the olefin and therefore the maximum of the total energy occurs when the olefin starts to displace the $\beta$-agostic bond. The smaller the metal ion, the earlier the displacement. The BS insertion path shows no such pronounced variations of the location of the transition state, since the $\beta$-agostic bond can be maintained at all times during insertion.

FS and BS insertion barriers for metallocene systems are surprisingly low, in fact they are usually lower than the barriers of sterically unencumbered systems. This might seem somewhat counterintuitive as one might expect that the steric congestion around the metal might pose an obstacle to the insertion process. However, in the light of our findings, this puzzle is solved easily: The bulky Cp ligands force the alkyl chain into planar arrangement (as already pointed out in part 1 of this study[34]), so that the deformation required to attain the insertion transition state is minor. The only obstacle to insertion is therefore the rupture of the agostic bond during FS insertion. As detailed in Part 1 of this study,[34] $\beta$-agostic rupture energies are generally lower than 20 kJ/mol and therefore the barriers have a comparable magnitude. It appears therefore that in general, steric encumbrance can serve as a means to lower the insertion barrier. Extreme steric encumbrance such as in bis-Cp systems

also serves to raise the energy of the BS transition state over the FS transition state despite the $\beta$-agostic stabilization being lost in the latter case. In contrast to sterically minimal systems $[L]MC_2H_5^{n+}$ (L = 7, 8, 9), the bis-Cp system has two well-defined insertion channels since chain rotation—which interconverts FS- and BS-TS—is impaired by steric bulk. In the BS insertion transition state, this gives rise to steric repulsion between the ethylene and alkyl fragments, since they cannot properly align with each other. Steric bulkiness of the auxiliary ligands that restricts torsional freedom of the alkyl also serves to cleanly separate FS and BS insertion pathways, which is important for stereoregular polymerization.

The fact that the insertion barriers for $[4]HfC_2H_5^+$ are very low (≈20−30 kJ/mol instead of ≈50−70 kJ/mol for sterically small systems with L = 7, 8, 9) teaches an essential lesson: even catalysts with metal centers that intrinsically have high barriers can be made very active by attaching appropriate steric bulk. It would seem that this allows the creation of catalysts with arbitrary $d^0$ metal centers and ligands, as long as there is tailored steric bulk which is able to compensate any deficiencies that arise from an intrinsically inactive core metal−ligand framework. Most recently, Cavallo et al.[70] have demonstrated that it is even possible to create a low insertion barrier for non-$d^0$ systems by using sterically bulky auxiliary ligands. In their special case, a Ti(III) $d^1$ center coordinated by 2 $MgCl_3^-$ bidentates exhibits a barrier of only 28 kJ/mol for insertion of ethylene into the Ti−ethyl bond.

**(d.3) Departure from Pseudo-$C_{2v}$ Symmetry of the [L]M Fragment.** If the auxiliary ligand set is not sufficiently close to $C_{2v}$ symmetry, new geometric variants (other than FS/BS) are created and the overall shape of the potential surface becomes more complex. In the following, we will investigate a few systems where $C_{2v}$ symmetry is violated. Ligand [10]—essentially the "living" system by McConville et al.[4] without steric bulk—is a simple modification of ligand [7], but has a propylene group bridging the amido ligands. System [11] is similarly related to ligand [8]. Both [10] and [11] have a puckered propylene bridging group that gives rise to exo−endo isomerism with respect to the orientation of the alkyl chain. However, the puckering is fairly far removed from the metal center so that [10] and [11] should behave similarly to the minimal ligands [7] and [8].

For ligand [10], we notice that FS insertion barriers do not rise substantially from Ti to Hf. It seems, therefore, that ligand [10] possesses properties which have the power to smooth out the otherwise sharp increase of insertion barriers from Ti to Hf (something that was also observed for the bis-Cp ligand). Ligand [10] constrains the amido groups to perfect planarity,[52] enforcing $\pi$-donation from the amido lone pair to the metal. This, it was concluded,[52] strongly enhances the preference for planar configuration and vice versa, diminishing the aptitude toward pyramidal arrangement. We have in section c shown that a strong preference for planarity decreases the FS insertion barrier and so it is not surprising that the FS insertion barrier for [10]Hf is lower than that for [7]Hf. We can test that hypothesis by exchanging ligand [10] for ligand [11], which has the same coordination geometry but a lessened $\pi$-donation ability. As expected, in this case the FS insertion barrier is much higher than that for ligand [10] and the rise with respect to the metal center is much sharper. Also, FS insertion is much disfavored over BS insertion. $\pi$-donor ligands that have the ability to enhance the preference for planar ligand arrangement have the effect of lowering the insertion barrier for heavy transition metals.

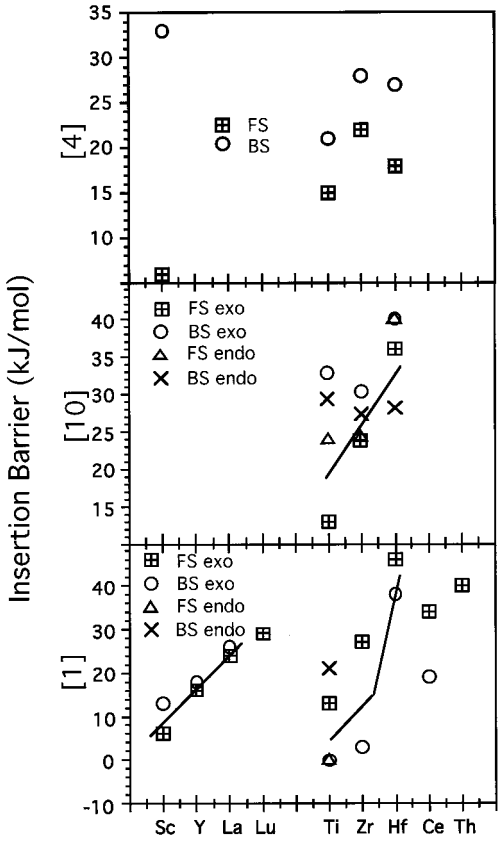


**Figure 4.** Insertion barriers for systems $[L]MC_2H_5^+$ with realistic ligands (L = 1, 4, 10) in units of kJ/mol. Lines are meant to show qualitative trends only. For systems with ligand [10] a propyl group was used to model the growing chain.

A more severe change from a $C_{2v}$ toward a $C_s$ symmetric [L]M fragment is represented by ligand [1], which has a bridging $\pi$-system that donates electrons to the metal. In contrast to ligand [10], the puckering here is strong and is expected to have effects on the electronic structure of the metal center. Furthermore, ligand puckering gives rise to pronounced exo−endo isomerism. We have calculated exo and endo, FS and BS transition states for [1]Ti. From our calculations on [1]Ti it seemed that by taking into account the exo pathway only, one could save considerably on CPU time while still getting a good idea of trends in barrier sizes and their spreads. Therefore, we calculated only species along the exo insertion pathway for Sc, Y, La, and Lu and Ti, Zr, Hf, Ce, and Th. Despite the strong deviation from $C_{2v}$ symmetry, these calculations yielded clear trends that coincide well with calculations on [7]M and [10]M. Moving down the triad increases the insertion barrier (FS as well as BS).

Trends discussed so far for realistic ligands are summed up in Figure 4, which shows that FS as well as BS insertion barriers increase as the aptitude of the metal ligand framework toward

(70) Cavallo, L.; Guerra, G.; Corradini, P. *J. Am. Chem. Soc.* **1998**, *120*, 2428.

(71) Consider a case where both $\pi$ complexes (FS and BS) insert through the same transition state TS, their absolute energies being $E_{FS}$, $E_{BS}$, and $E_{TS}$. To show that the observed rate constant $k_{obs}$ is markedly diminished by the higher one of the two activation barriers when the steady-state condition $c_{BS}/c_{FS} = \exp[-(E_{BS} - E_{FS})/RT]$ applies, a limiting scenario where $E_{BS} = E_{TS} > E_{FS}$ can be used. Here, $k_{obs}(c_{FS} + c_{BS}) = c_{FS} \exp[-\Delta E^{\ddagger}_{FS}/RT] + c_{BS} \exp[-\Delta E^{\ddagger}_{BS}/RT]$ ($\Delta E^{\ddagger}_{FS} = E_{TS} - E_{FS}$; $\Delta E^{\ddagger}_{BS} = E_{TS} - E_{BS} = 0$). Therefore, the observed rate constant $k_{obs} = 2 \exp[-\Delta E^{\ddagger}_{FS}/RT]/(1 + \exp[-\Delta E^{\ddagger}_{FS}/RT])$. One can see that the rate of polymerization is significantly retarded as $E_{FS}$ drops and $\Delta E^{\ddagger}_{FS}$ increases. Note that $c_{FS}$ and $c_{BS}$ stand for the total concentrations of all FS and BS $\pi$-complexes, respectively, regardless of the length of the growing alkyl chain.

planar configuration diminishes. Following this trend, which was outlined in part 1 of this study, the insertion barriers increase in the order Sc < Y < La < Lu and Ti < Zr < Th < Hf and are generally lower for group 3 metals than for group 4 metals. This permits—as long as there is approximate $C_2$ symmetry of the [L]M framework—the prediction of the intrinsic activity of a given $d^0$ ethylene polymerization catalyst from the knowledge of its aptitude toward planar configuration and also the tuning of catalyst activity by skilled metal and auxiliary ligand variation.

To verify our supposition that (a) basically any $d^0$ complex is able to catalyze olefin polymerization and that (b) this intrinsic ability can be enhanced by sterically compressing the active site, we use the *acac*-derivative complex $[6]VC_2H_5^+$. This system is sterically rather constricted since the $V^{5+}$ ($d^0$) cation is small and the available space is largely taken up by the auxiliary ligand set and the alkyl chain. Our calculations show that this complex can indeed insert ethylene into the M−$C_\alpha$ bond, with activation barriers of 5 (FS) and 4 (BS) kJ/mol. Here, the nomenclature of FS and BS attack has been transferred to a situation where there is no approximate $C_2$ symmetry. However, the attack of the ethylene can proceed either syn or anti to the $\beta$-agostic bond of the precursor complex, so that the expressions FS and BS can be applied to the syn- and anti-attack, respectively.

## Concluding Remarks

We have presented a systematic survey of the barrier of ethylene insertion into transition metal−alkyl bonds for a number of complexes of $d^0$ and $d^0f^n$ metals (M = Sc(III), Y(III), La(III), Lu(III), Ti(IV), Zr(IV), Hf(IV), Th(IV), and V(V)). A number of ligands (L = NH-$(CH)_2$-$NH^{2-}$ [1], N$(BH_2)$-$(CH)_2$-$(BH_2)N^{2-}$ [2], O-$(CH)_3$-$O^-$ [3], $Cp_2^{2-}$ [4], NH-Si$(H_2)$-$C_5H_4^{2-}$ [5], [(oxo)(O-$(CH)_3$-O)]$^{3-}$ [6], $(NH_2)_2$ [7], $(OH_2)_2$ [8], $(CH_3)_2^{2-}$ [9], NH-$(CH_2)_3$-$NH^{2-}$ [10], and O-$(CH_2)_3$-$O^{2-}$ [11]) have been attached to these metal centers to elucidate the influence of different ligand−metal combinations upon olefin insertion barriers. We have found that olefin insertion barriers for all $d^0$ complexes are (a) generally small due to a lack of metal d electrons which could fill an emerging carbon−carbon antibonding interaction in the insertion transition state. (b) Insertion barriers are smallest for metal−ligand combinations which have a high intrinsic aptitude for planar arrangement, such as light transition metals (Sc, Ti) ligated by good $\pi$-donor ligands such as amido ligands. (c) Large steric bulk facilitates insertion by favoring the insertion transition state if it restrains the metal−ligand framework to a planar arrangement. (d) Our results provide means to manipulate insertion barriers by changing the metal, the donor atoms of the auxiliary ligands, and the steric bulk of the auxiliary ligand. Steric modeling can be used to override intrinsic limitations imposed by the metal ion and the first coordination sphere of the auxiliary ligands. (e) The results obtained in this study can be extrapolated to complexes with nonzero d occupations: if the metal d orbitals are high enough in energy to donate electrons into the olefin $\pi^*$-orbital and have the right symmetry, the carbon−carbon antibonding interaction in the transition state will be occupied, which in turn will create an electronic barrier for the insertion process.

**Acknowledgment.** This work has been supported by the National Sciences and Engineering Research Council of Canada (NSERC), as well as by the donors of the Petroleum Research Fund, administered by the American Chemical Society (ACS-PRF No 31205-AC3). P.M. acknowledges fruitful discussions with T. K. Woo and R. Schmid.

**Supporting Information Available:** A listing of Cartesian coordinates and atomic basis sets used as well as a plot of the orbitals relevant for olefin insertion into the M−C bond of [1]-$ScC_2H_5$ (7 pages, print/PDF). See any current masthead page for ordering information and Web access instructions.

JA9742139